Single Crystal Silicon (SCS) XY-Stage Fabricated by DRIE and IR alignment

Chris S.B. Lee, Sejin Han and Noel C. MacDonald
School of Electrical Engineering
Cornell University, Ithaca NY14853
aloha@ee.cornell.edu, (tel) 607-255-8026

Abstract

We describe a two-depth, large displacement, highly linear motion, SCS XY micro-positioning stage fabricated by Deep Silicon Etching and IR front-to-back alignment. A positioning range of up to 160 μm by 160 μm in the xy plane has been achieved. In order to release a large, SCS flat stage, IR alignment is used to open an etch window from the back of wafer. The device has a 400 μm by 300 μm SCS stage suspended by 14 μm springs and actuated by 100 μm deep comb fingers.

Introduction

Previously, we have reported the results of two depth, single crystal silicon (SCS) comb-drive actuator for large displacements fabricated by Deep Silicon Etching (Bosch silicon Process). Displacement of 130 μm at 37 volts was achieved with a 12 mm^2 comb-drive actuator. The height of fingers and springs are 100 μm and 22 μm, respectively [1,2], and are shown in Figure 1. A natural extension of a large displacement actuator is the construction of a large displacement xy-stage, where we are interested in large linear motion, accurate xy positioning, scanning and detection technology. The potential energy that is stored by a pair of comb electrodes is given by,

$$u = \frac{1}{2}\int \varepsilon E^2 dv \qquad (1)$$

where E is the electric field across the plates, ε is the dielectric constant, and v is the volume of capacitor. The stored energy is related to the force using the following first-order differential equation, where the actuation is assumed in the y direction.

$$F = -\frac{\partial u}{\partial y} \qquad (2)$$

Relate the force to the comb finger geometry,

$$F = \frac{n\varepsilon h_s}{g} V^2 \qquad (3)$$

where g is the finger gap, h_s is the height of the fingers, and V is the applied voltage.

The underlying principles of the two-depth actuator and its impact on displacement can be easily seen by (4). The displacement is derived as a function of the applied voltage and the parameters for the finger geometry using the Hook's law,

$$y = \frac{n\varepsilon h_f}{k_y g} V^2 = \frac{n\varepsilon}{2Eg}\left[\frac{h_f}{h_s}\right]\left[\frac{L_s}{b_s}\right]^3 V^2 \qquad (4)$$

$$k_y = \frac{2Eh_s a_s^3}{L_s^3}$$

where y is the displacement in the direction of actuation, n is the number of comb fingers, h_f is the height of the comb fingers, h_s is the height of the springs, g is the comb finger gap, k_y is the folded spring constants in the y direction, L_s is the length of the springs, a_s is the width of springs, E is the elastic modulus of the system, and V is the applied voltage.

With a fixed finger gap and die size, there are two ways to increase the displacement of the actuator. As indicated in the equation, the displacement increases proportional to V^2 and $[L_s/b_s]^3$. However, there are some disadvantages associated with increasing these parameters. Increasing the voltage is not desirable because it will speed the breakdown of the dielectric and require a high voltage power source. Second, there are some physical limitations associated with increasing the ratio of $[L_s/b_s]^3$. For example, the reduction of the spring width is limited to one's pattern generating capability and by process control for preserving the verticality of the etching recipe. Also, increase in the length of the springs increases the overall dimension of the device size, and the planarity of the springs [3] also becomes more difficult to control due to the thermal stress.

A new proposed approach is to make the ratio of h_f (the height of fingers) to h_s (the height of the springs) significantly greater than one using only a single photolithography step on a standard silicon substrate,

while optimizing the ratio of $[L_s/b_s]$. The important advantage of the two-depth process is that it results in a ratio substantially greater than one while maintaining a simple fabrication flow. Without any changes in the CAD design, the benefits of larger displacement and higher force can be achieved by increasing κ where it is defined by

$$\kappa = \frac{h_f}{h_s} \qquad (5)$$

(a)

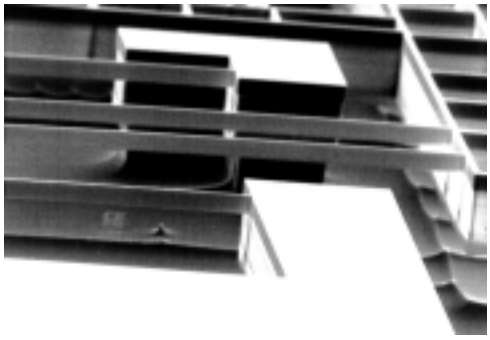

(b)

Figure 1. (a) Representative image of two-depth actuator with a 22 μm deep spring integrated into the deeper fingers and backbone. (b) A close-up view. Here, the height of the fingers is 100 μm. The two-depth process requires only one photolithography step and a standard silicon wafer.

An upper bound of κ exists, and it is largely dependent on the actuator design and the process control of the deep silicon etching process. As κ increases, the torsional levitation during the in-plane actuation also increases. Due to a large moment of inertia and stiff backbone structure, the torsional levitation is measured below 50 nm at 30 volts in both quasi DC conditions and AC conditions below the KHz range. This is less than 0.05 % of the corresponding in-plane displacement. The motion can be further suppressed by an optimum actuator design.

The Bosch silicon etching process also influences the upper bound of κ. As the aspect ratio of structures becomes greater by deeper etching, the etch rate of silicon is reduced significantly, and the profile control may become difficult [4,5,6]. This will ultimately dictate the maximum finger depth within the stable actuation range.

Design of Large Motion Actuators

The maximum displacement of a comb-drive actuator is bounded by the electromechanical lateral instability of the fingers. A reliable design for stable actuation must be based on a model of comb finger stability [7,8]. Such a design prevents the movement of the fingers in the direction perpendicular to the stroke direction, preventing a short circuit between the fixed and movable fingers. In this section, the stability analysis of the two-depth actuator is derived. The result of the analysis provides a basis for determining the actuator dimensions.

The movable actuator-fingers are designed to be centered between the fixed fingers. Any deviation from perfect symmetry will cause an asymmetrical electrostatic force F_x generated by both sides of the parallel plates. Here, the direction of actuation is in the y direction. For stable operation, the spring constant in the axial direction needs to be large enough to overcome the instability of F_x:

$$\frac{\partial F_x}{\partial x}\Big|_{x\to 0} < k_x \qquad (6)$$

$$\frac{2n\varepsilon h_f (y_0 + y)}{g^3} V^2 < \frac{2Eb_s h_s}{L_s} \qquad (7)$$

where k_x is the stiffness of the spring system in the axial direction, y_0 is the initial finger overlap, and $y+y_0$ is the effective comb finger length. At a critical voltage, V_{cr}, the inequality no longer holds, and the lateral instability causes the movable fingers to contact the fixed fingers after overcoming the axial stiffness of the springs. The critical voltage can be found by equating the left-hand side and the right hand side of (7):

$$V_{cr}^2 = \frac{E}{n\varepsilon}\left[\frac{b_s}{L_s}\right]\left[\frac{h_s}{h_f}\right]\frac{g^3}{(y_0 + y)} \qquad (8)$$

Substituting V_{cr} into equation (4), the corresponding critical displacement, y_{cr}, is obtained

$$y_{cr}^2 + y_0 y_{cr} = \frac{g^2}{2}\left[\frac{L_s}{b_s}\right]^2 \qquad (9)$$

A real solution to the quadratic equation is

$$y_{cr} = g\sqrt{\frac{y_0^2}{4g^2} + \frac{k_x}{2k_y}} - \frac{y_0}{2} \qquad (10)$$

But,

$$\frac{y_0^2}{4g^2} << \frac{k_x}{k_y}$$

Therefore,

$$y_{cr} \approx g\sqrt{\frac{k_x}{2k_y}} - \frac{y_0}{2} \qquad (11)$$

(11) indicates that actuators with smaller finger gaps will become unstable at smaller displacements than those with larger gaps, and the actuators become more unstable as the overlap length increases. Also, the instability is shown to increase with higher applied voltage because the spring constant of the folded flexure in the x direction decreases with increasing beam displacement in the y direction. The design parameters for the two-depth actuators are presented elsewhere [1].

Design of the XY stage

The suspended flat stage is driven by a set of four large-displacement actuators. Each actuator is positioned at 90 degrees with respect to the adjacent actuator. The actuators are designed to pull the micro-stage along the axis**.** The overview of the device is shown in Figure 2.

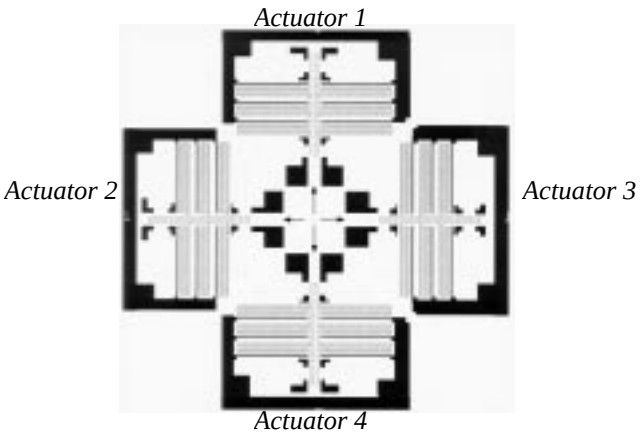

(a)

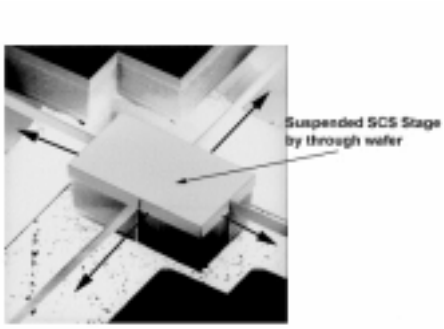

(b)

Figure 2. (a) The overview of xy stage configuration. The stage is positioned at the center of device, and designed to be pulled by appropriate actuators. The coupling springs are the mechanical beams that connect the suspended structures of the device. (b) A close up view of the suspended SCS stage.

The xy stage design is based on the mechanical coupling of the four units of two-depth actuators using coupling beams. The analysis of motion decoupling is given in a later section.

Positioning of up to 160 μm by 160 μm in the xy plane at 30 volts is designed. In order to release a large SCS flat stage, a front-to-back alignment is used to open an etch window from the back. A 400 μm by 300 μm SCS stage is driven by four sets of comb-actuators where the springs are 14 μm deep and the fingers are 100 μm deep. The two-depth configuration gives the benefit of a large electrostatic force and a compliant spring to obtain a large displacement per unit of actuator force. The other actuator parameters are given in Table 1. The off-axis displacement is possible by energizing two adjacent actuators simultaneously. The entire fabrication requires two masks. Due to the stiff backbone design and the large moment of inertia, the torsional levitation during the in-plane actuation has been measured and shown to be negligible in both DC and AC excitations.

Together with nanotools such as microtips, an integrated system can be conceptualized on the flat stage.

Fabrication

The detailed fabrication sequence for the two-depth actuator has been presented previously [1]. The same fabrication flow can be used if the stage design is a grid structure. For a solid stage, a front-to-back alignment is required to open the through-the-wafer etch window from the back of wafer. The process flow of through-the-wafer module is described in Figure 3.

1. Double Sided Polished Wafer
2. Defining the through-the-wafer etch window on back of wafer.
3. Fabrication of two-depth structures on the front of wafer. Patterns are aligned to back using IR aligner.

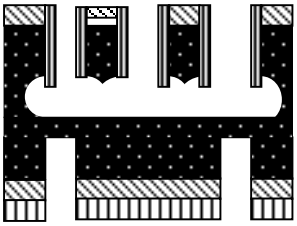

4. PECVD oxide deposition: Etch stop layer (100 nm)
5. Through-the-wafer etch from back

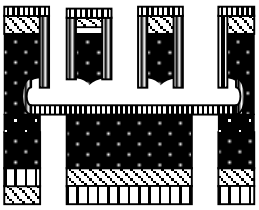

6. CHF_3 oxide etch to remove the etch-stop layer
7. Al metallization.

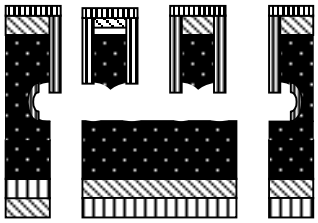

Figure 3. Process flow for xy stage

Characterization of two-depth actuators

The quasi-static displacement of a two-depth actuator was measured for static displacement using laser vibrometry [9]. The location of the on-chip mirror is shown in Figure 4. A quasi-static ramp-function input was applied to the actuator using a HP 8116 Pulse/Function Generator. A plot of displacement versus applied voltage squared is shown in Figure 5. The maximum measured displacement is 40 μm. The vibrometer output signal beyond 40 μm of displacement deteriorated significantly for these quasi DC measurements. The figure indicates that the motion is highly linear, and the extracted value for the linear spring coefficient is listed in Table 2.

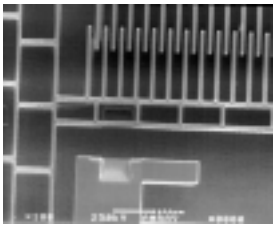

Figure 4 Scanning electron micrograph of 45-degrees FIB (Focus Ion Beam) milled mirror and a moving actuator arm.

Number of Fingers	310
Heights of Fingers	100 μm
Width of Fingers	6.0 μm
Finger Gap in CAD	14.5 μm
Length of Springs	1100 μm
Heights of Springs	14.0 μm
Width of silicon Springs (CAD)	2.0 μm
Length of Backbone	3500 μm
Heights of Backbone	100 μm
Initial Finger Overlap	30.0 μm

Table 1. The actuator design parameters for the xy stage.

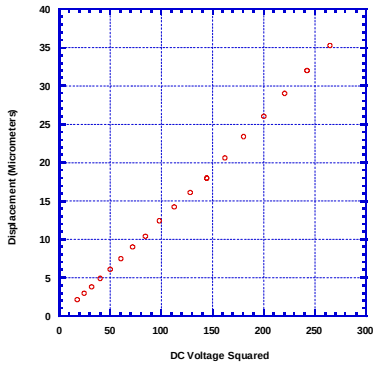

Figure 5. A plot of displacement versus DC voltage squared using the laser vibrometer technique. A quasi-static ramp-function was used. The motion of two-depth actuator is shown to be highly linear. The measurement is read from oscilloscope.

In order to extract other relevant actuator parameters, the dynamic response of device was measured. A sinusoidal input voltage was generated using a HP3324A signal generator. A sinusoidal voltage was applied for each sweep. Figure 6 indicates that the resonant frequency of device is approximately 240 Hz. Based on the methology presented by Turner et. al [9], the shape of frequency response plot is used to obtain parameters such as Quality factor, cubic spring constant, resonant frequency, mass, and actuator factor. The frequency response plot is shown to be very symmetrical, indicating a highly linear system which is consistent with previous plots. In comparison to the data presented by Turner, the nonlinear cubic term is

several orders less for our devices because of the compliant spring design.

Quality Factor	8.3
Linear Spring Constants	0.123 N/m
Cubic Spring Constants	4.53 x10^2 N/m^3
Resonant Frequency	238.4Hz
Mass of suspended structures	5.454 e-8Kg
Actuator Factor	0.131 μm/V^2

Table 2. The extracted two-depth actuator parameters for the xy stage from the frequency response plot.

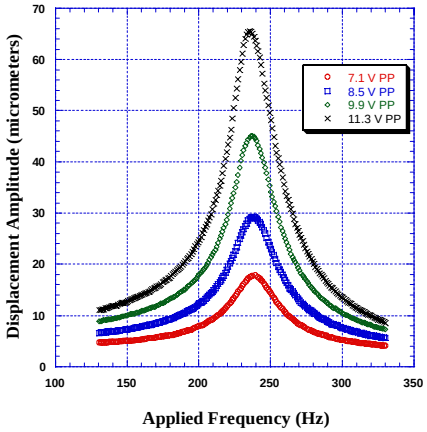

Figure 6. Displacement amplitude versus frequency in air. The plot is symmetric, indicating a linear spring coefficient. The measurement was obtained with frequency spectrum analyzer.

Decoupling of Motion

For positioning devices, it is important to control the two moving directions independently. The concept of motion decoupling is considered in the context of the layout shown in Figure 2(a). A large displacement in the positive *y*-direction results from applying voltage to actuator 1. Since the suspended structures of the actuators are connected to each other, it is important to ensure that the suspended structures on the x-actuators (actuators 2 and 3) remain in their equilibrium position. If not, the movable fingers will no longer be centered between the fixed fingers, and this will accelerate side stability failure as the voltage is applied to the x-actuators for the off-axis movement of the stage. The device is designed so that deflections in one direction induce minimal unwanted movements in the orthogonal directions.

The coupling influence is simulated using ABAQUS. The result of the simulation is shown in Figure 7. When the stage travels 80 μm in the positive *y*-direction, less than 1 nm of motion is induced on the movable parts of the x-actuators. Such a negligible motion results from a large axial stiffness of the folded springs in the x-actuators. Equation (12) shows the calculation of the axial stiffness. A factor of four is included in the calculation since there is a total of four folded springs in the x-axis. For the x-actuators to have any induced motion due to the y-displacement, the suspended structures have to overcome a high axial stiffness shown in (12). A composite modulus for the spring is used in the calculation.

$$K_{axial} = \frac{4 \cdot 2(90Gpa)(14x10^{-6}\,m)(2.0x10^{-6}\,m)}{(1100x10^{-6}\,m)} \qquad (12)$$
$$= 18330 N/m$$

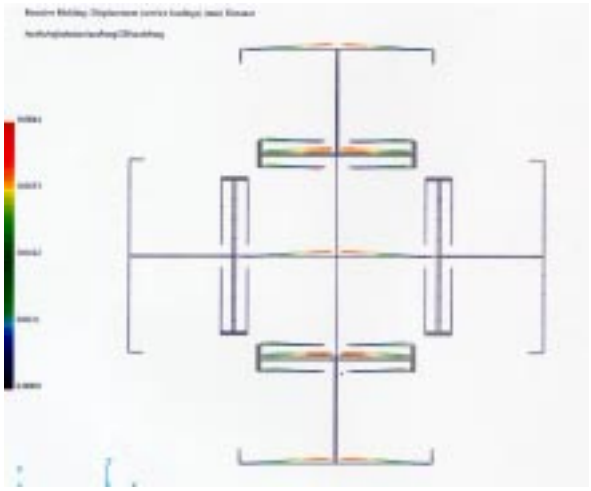

Figure 7. Representative simulation result of axis decoupling. The y-motion is induced on the stage using the actuator 1. The actuator 4 follows the motion. The x-actuators remain in its equilibrium position because of very high axial stiffness of its folded springs.

The coupling influence of current design is simulated using ABAQUS. FEM simulations showed that precise positioning can be performed because there is a good common-mode rejection ratio of the displacements in the x and y directions [10]. This is consistent with the vibrometer measurement. Four on-chip mirrors are milled at the vicinity of xy stage. While the stage is traveling in the y-direction, the laser is focused on the mirror that is facing the stage in the x-direction. The output of trace is shown in Figure 8. Here the actuator-1 is supplied with 40 V at 100 Hz. No corresponding movement in the x-direction is observed over the 10 nm of noise level.

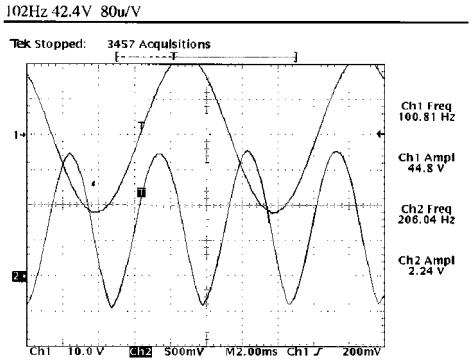

(a)

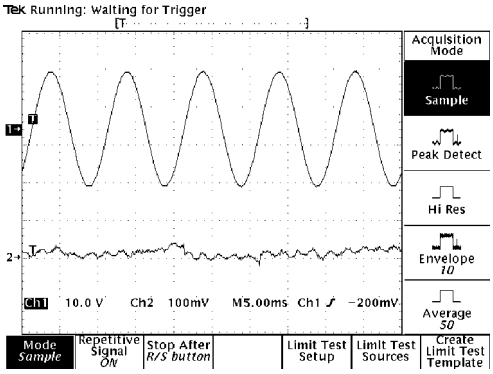

(b)

Figure 8. (a) The vibrometer output when the stage is making a large positive y-motion. The scale of vibrometer is at 80 μm/V. The stage is moving 160 μm. (b) The vibrometer output for the x-direction when the stage is still making a large y-motion. The scale is set at 1 μm/V.

Conclusion

Two-depth, large displacement, a highly linear motion, SCS XY micropositioning stage was fabricated by using the deep silicon etching and IR alignment. A 400 μm by 300 μm SCS stage is driven by four sets of comb-actuators. Individual actuators have been characterized by laser vibrometry. The motion decoupling is measured to be negligible. Positioning of up to 160 μm by 160 μm in the xy plane has been measured. In order to release a large SCS flat stage, a front-to-back alignment is used to open an etch window from the back of wafer.

Acknowledgments

This work is supported by DARPA. All the fabrication was performed at the Cornell Nanofabrication Facility (CNF) which is supported by the NSF, Cornell University, and Industrial affiliates. The authors would like to thank Prof. MacDonald's group members for their generous support of this research.

Reference

1. C.S. Lee, S. Han, and N.C. MacDonald, "Multiple Depth, Single Crystal Silicon MicroActuators For Large Displacement Fabricated by Deep Reactive Ion Etching". 1998 Solid-State Sensors and Actuators Workshop, Hilton Head Island, SC, 45-50.
2. W. Hofmann, C.S. Lee, and N.C. MacDonald, "Monolithic Three-Dimensional Single-Crystal Silicon Microelectromechanical Systems", Sensors and Materials, Vol. 10, No. 6, 1998, 337-350.
3. M.T.A. Saif and N.C. MacDonald, "Planarity of Large MEMS", J. Microelectromech. Syst. 5, 1996, 79-97.
4. R.A. Gottscho, C.W. Jurgensen and D.J. Vitkavage, "Microscopic uniformity in plasma etching", J. Vac. Sci. Technology B, 10(5), 1992, 2133-2147.
5. Y.H. Lee and Z.H. Zhou, "Feature-Size Dependence of Etch Rate in Reactive Ion Etching", J. Electrochem. Soc. Vol. 138, No. 8, 1991, 2439-2445.
6. A.A. Ayon et al., "Etching Characteristics and Profile Control in a Time Multiplexed Inductively Coupled Plasma Etcher", Solid-State Sensor and Actuator Workshop, Hilton Head Island, SC, 1998, 41-44.
7. R. Legtenberg, A.W. Groeneveld, and M.Elwenspoek, "Comb-drive actuators for large displacement", J. Micromech. Microeng., 6, 320-329.
8. T. Hirano, T. Furuhata, K.J. Gabriel, and H. Fujita, "Design, Fabrication, and Operation of Submicron Gap Comb-Drive Microactuators", J. Microelectromech. Syst. 1, 52-58.
9. K. Turner, P. Hartwell, and N.C. MacDonald, "Mult-Dimensional MEMS Motion Characterization using Laser Vibrometry", Transducers 99, 1144-1147, Sendia Japan
10. V.P. Jaecklin, C. Linder and N.F. de Rooij, "Comb actuators for xy-microstages", Sensors and Actuators, A-32 (1993), pp. 83-88.